Published in final edited form as:
J Magn Reson Imaging. 2014 November ; 40(5): 1230–1237. doi:10.1002/jmri.24479.

Estimation of the Absolute Shear Stiffness of Human Lung Parenchyma using ^{1}H Spin Echo, Echo Planar Magnetic Resonance Elastography

Yogesh K Mariappan, Ph.D[1], **Kevin J Glaser, Ph.D**[2], **David L Levin, MD, Ph.D**[2], **Robert Vassallo, MD**[3,5], **Rolf D Hubmayr, MD**[4,5], **Carl Mottram, R.R.T**[4], **Richard L Ehman, MD**[2,5], and **Kiaran P McGee, Ph.D**[2,*]

[1]Philips Healthcare, Bangalore, Karnataka, India

[2]Department of Radiology, Mayo Clinic, Rochester, MN, USA

[3]Department of Medicine, Mayo Clinic, Rochester, MN, USA

[4]Department of Pulmonary and Critical Care Medicine, Mayo Clinic, Rochester, MN, USA

[5]Department of Physiology and Biomedical Engineering, Mayo Clinic, Rochester, MN, USA

Abstract

Purpose—To develop a rapid proton MR Elastography (MRE) technique that can quantify the absolute shear stiffness of lung parenchyma, to investigate the ability to differentiate respiration-dependent stiffness variations of the lung, and to demonstrate clinical feasibility.

Methods—A spin-echo echo planar imaging MRE sequence (SE-EPI MRE) with a very short echo time was developed and tested in a series of 5 healthy volunteers at 3 different lung volumes: 1) residual volume (RV), 2) total lung capacity (TLC), 3) and midway between RV and TLC (MID). At each volume, lung density was quantified using a MR-based density mapping sequence. For reference, data was acquired using the previously described spin-echo lung MRE sequence (SE-MRE). MRE data was also acquired in a patient with proven Idiopathic Pulmonary Fibrosis (IPF) to test clinical feasibility.

Results—The SE-EPIMRE sequence reduced total acquisition time by a factor of 2 compared to the SE-MRE sequence. Lung parenchyma median shear stiffness for the 5 volunteers quantified with the SE-EPI MRE sequence was 0.9 kPa, 1.1 kPa and 1.6 kPa at RV, MID and TLC, respectively. The corresponding values obtained with the SE-MRE sequence were 0.9 kPa, 1.1 kPa and 1.5 kPa. Absolute shear stiffness was also successfully measured in the IPF patient.

Conclusion—The results indicate that stiffness variations due to respiration could be measured with the SE-EPIMRE technique and were equivalent to values generated by the previously described SE-MRE approach. Preliminary data obtained from the patient demonstrates clinical feasibility.

[*]**Correspondence** Kiaran P McGee Ph.D., Department of Radiology, Mayo Clinic, 200 First Street SW, Rochester, MN 55905, Phone: (507)-284-9770 Fax: (507)-284-9778 mcgee.kiaran@mayo.edu.

Keywords

Magnetic Resonance Elastography; Lung MR Elastography; Shear stiffness; Lung fibrosis; interstitial lung disease

Introduction

For over 40 years pulmonary physiologists have understood the central role of the mechanical properties of the lung in defining form and function and that this property undergoes significant alteration across a spectrum of lung diseases [1, 2]. For example, in obstructive lung diseases such as emphysema shear stiffness decreases (the lung becomes soft), while in restrictive lung diseases such as pulmonary fibrosis, parenchymal stiffness is known to increase (the lung becomes stiffer). More recent data have confirmed this relationship and provided evidence that the change in mechanical properties of lung parenchyma *precede* the initiation and promotion of certain lung diseases [1]. While conventional imaging techniques, most notably CT [3], provide excellent discrimination of structural morphology they are unable to non-invasively quantify and spatially resolve the intrinsic mechanical properties of the lung [4].

Magnetic resonance elastography (MRE) is a recently developed phase-contrast MRI method for quantifying the topographical distribution of shear stiffness of soft tissues [5]. Because of the central role of tissue stiffness in many disease processes, MRE is being investigated as a diagnostic tool for several solid organ diseases [6–17] and within our own institution is rapidly replacing biopsy as the reference standard for the assessment of hepatic fibrosis [18].

This technique also has significant potential for applications within the lung. However lung MRE is technically challenging, due primarily to the low MR signal of the lungs as a result of the decreased lung tissue density (~1/3rd of solid organs) and an ultra-short T_2* (in the range of 1–3 ms [19]). The need for MRE-specific motion-encoding gradients increases the minimum achievable echo time of MR pulse sequences, further reducing the lung MR signal. Consequently, phase-contrast (i.e. MRE) images of the lungs are typically dominated by noise. In addition, respiratory- and cardiac-induced motion can create significant motion artifacts, requiring the use of breath-holds and/or ECG gating techniques. While experiments with exogenous contrast agents such as hyperpolarized Noble gases have successfully demonstrated that a several fold increase in signal can be achieved [20–23], their dwindling supply [24], the need for dedicated and expensive MR hardware, and the necessary technical expertise to use these agents suggest that their clinical application is limited. What is needed is a more practical proton-based technique for imaging lung mechanical properties.

It has been recently demonstrated that propagating shear waves can be visualized within human lungs with modified spin echo pulse sequences and that density-dependent parenchymal shear stiffness can be spatially resolved in vivo [25, 26]. While these results are promising, the single-echo spin echo MRE approach has the limitations of relatively long acquisition times making clinical implementation challenging. It is possible to adapt this sequence into a respiratory triggered free breathing sequence but with a penalty of

further increasing acquisition time. In addition, due to the long T_1 of the lung parenchyma (~1,300 ms [19]) and the relatively short repetition time (TR) of the spin-echo sequence (200 ms, [25]), longitudinal magnetization recovery was limited resulting in a low MR signal. We hypothesized that the acquisition speed of pulmonary MRE sequences can be increased by development of a spin echo echo planar imaging (EPI) MRE pulse sequence without significant loss of SNR compared to the conventional spin echo sequence. The objective of this work was to test this hypothesis in combination with a gradient echo-based localized density estimation sequence for spatially resolving the absolute shear stiffness of lung parenchyma and to evaluate the ability of this technique to measure respiration-dependent stiffness variations within the lungs in healthy volunteers and a patient volunteer.

Methods

Echo Planar Imaging based Faster Imaging

Previous efforts have reported on repetition time and total acquisition times of a single-echo spin echo lung MRE acquisition of 200 ms and 64 seconds for four phase offsets [25] respectively, with each phase offset data acquired in sequential breath-holds of 16 seconds (Figure 1a, [25]) each. In this work, a ^{1}H SE-EPI based MRE sequence with an echo train length of 8 and a minimum achievable TR of 320 ms was developed. Specific features included fractional motion encoding [27], split motion-encoding gradients and crusher gradient removal as described for spin echo pulmonary MRE in [25]. In addition, the sequence included two 2-ms unipolar motion-encoding gradient (MEG) lobes for encoding propagating shear wave induced displacements. To minimize the TE, slice selection was performed with a simple slice-selective pulse (rather than a spatial-spectral pulse). A chemical presaturation pulse was included to saturate the fat signal. The TE of this sequence was 11.7 ms and a pulse sequence diagram (PSD) of this modified sequence is shown in Figure 1b. These modifications allowed for a minimum TR of 320 ms and for a reduction of overall scan time without increasing the breath-hold duration. The consequence of the increased TR is an increase in T_1-dependent signal recovery. The total scan time could be reduced, compared to the single echo spin echo sequence by a factor of 2 to 30 s, split into two breath-holds of 15 s each.

Density Estimation

A simple form of the working equations for MRE inversion can be written as

$$\mathrm{as}\mu=\rho V_s^2 \quad \text{(e1, [28])}$$

where μ is the shear stiffness, ρ is the physical density of the tissue of interest and V_s is the shear wave speed. While the shear wave speed is measured by studying shear wave propagation in the MRE phase or wave images, MRE inversions typically assume ρ to be equal to 1 g/cm^3 (equal to that of water). Stiffness values obtained with this density assumption will be referred to as an “effective stiffness” in this work. For the majority of soft tissues this is a reasonable assumption. However, this no longer holds for the lung due to the fact that the density of the lung is approximately 1/3rd to 1/4th that of solid organs [29], spatially heterogeneous and varies significantly through the respiration cycle. Accurate

spatial resolution of lung shear stiffness therefore requires mapping of lung tissue density. Towards this end, a fast gradient recalled echo lung density estimation (FGRE-LDE) pulse sequence similar to the one described in [29, 30] was developed. This method involves the acquisition of 12 images but with just two distinct interleaved TE values (1 ms and 1.8 ms), with a typical TR value of 15 ms, within a single breath-hold of 13 seconds. From these 12 images, due to signal equilibrium concerns, the first four images are discarded and 2 mean magnitude images for the two TE values are calculated from the remaining 8 images. From these average images, physical density can be calculated by fitting a mono exponential decay equation

$$I_j = I_0 e^{\left(\frac{t_j}{T_2^*}\right)} \quad \text{(e2, [29])}$$

where I_j is the average signal for a particular TE, I_0 is the T_2* independent MR signal, t_j is the TE value (either 1.0 ms or 1.8 ms), and T_2* is the relaxation constant of the lung parenchyma. To spatially resolve lung density, I_0 is first calculated and then normalized by the signal within a gadolinium-doped water phantom simultaneously imaged with the sample to provide a reference density. Additional information on this validated method is available in [29, 30]. The diagram of this sequence with a TE of 1.0 ms is shown in figure 1c.

Validation study

It is well known that the shear modulus of lung parenchyma increases during inspiration. To determine whether the proposed EPI lung MRE technique can differentiate these respiratory induced stiffness changes and in doing so provide an estimate of the sensitivity of the method, a series of experiments were performed on five healthy volunteers. MRE acquisitions were conducted both at maximum voluntary end expiration (i.e. Residual volume, RV) and at maximum voluntary end inspiration (i.e. Total lung capacity, TLC). A third respiratory state midway between RV and TLC (MID) was also measured. This was performed with the help of a spirometer (Easy on Pc, ndd Medical Technologies, Inc., Andover, MA) and an interactive breath-hold control device (IBC, Medspira, USA) connected to the respiratory bellows placed around the volunteer. Since the spirometer was not MR compatible, the volunteer was trained and the IBC was calibrated outside the scanner room. This included three steps:

1. The vital capacity of the volunteer was measured as the difference between the maximum voluntary inspiration (TLC) and maximum voluntary expiration (RV) breath hold levels. The blue line in figure 2b shows the spirometer tracing obtained from this step.
2. The volunteer was asked to take a full breath and was trained to hold their breath after blowing out half of their vital capacity (this state will be referred to as MID). The interactive breath-hold device, which can provide a visual feedback to the volunteer in the scanner, was calibrated to this MID state.
3. To test the reproducibility of this state, the volunteer was then asked to hold their breath based on the feedback from the IBC and the spirometer readings were

recorded. The red and the green lines show the spirometer tracings from steps 2 and 3 respectively, and it can be seen that the MID levels reached at these two steps were similar.

The validation study included the collection of MRE data at all three states of lung inflation (RV, MID, TLC) in five healthy volunteers (All male, age range: 23 to 51 years) with both the single-echo spin echo MRE pulse sequence (SE-MRE) and the newly developed EPI MRE pulse sequence (SE-EPI MRE). In addition to the MRE data, data were also collected for the assessment of density at these three states.

Data Acquisition and Analysis

All experiments were performed on a 1.5-T whole-body MR (Signa Excite, GE Healthcare, Waukesha, WI) scanner and were conducted after obtaining approval from the Institutional Review Board and written informed consent from the subject. Typical data acquisition parameters were: axial imaging plane, whole body RF coil for data acquisition, 48-cm FOV, 128×64 acquisition matrix, 128×128 reconstruction matrix, superior-inferior (SI) motion sensitizing direction, full FOV in the phase-encoding direction for EPI MRE (0.6–0.8 fractional phase FOV for SE MRE), TR/TE = 320/11.7 ms (200/9.4 ms for SE MRE), 40 mT/m MEG amplitude, four 15-mm slices and 4 phase offsets. The frequency-encoding direction was chosen to be in the right-left direction so that the cardiac motion artifacts would not significantly affect the lung MRE data.

Continuous 50-Hz shear vibrations were induced within the lungs using the pressure-activated driver system described in [18]. Figure 2a schematically shows the experimental setup and the location of the passive driver on the anterior chest wall of the right lung is indicated. In this study, only the right lungs were analyzed due to the presence of cardiac motion artifacts within the left lung. The passive driver couples the longitudinal vibrations created by the active driver to the lung tissue, where they undergo mode conversion generating shear waves that can be imaged with the MRE pulse sequence. A direct inversion of the Helmholtz equation describing the wave propagation [28] with spatio-temporal directional filters [31] was used to calculate the complex stiffness maps using sliding circular 11×11-pixel kernels. The complex stiffness was then converted to shear wave speed and reported in “effective stiffness” maps in units of kPa. The inversion algorithm also reported a confidence map based on the correlation coefficient of polynomial fits performed over the processing kernel and a threshold value of 0.7 was used to differentiate between regions of reliable and unreliable shear wave data. Density-independent shear stiffness maps were then calculated as the product of these effective stiffness maps and the density maps obtained from the density-estimation processing [29] and these stiffness maps will be referred to as “absolute stiffness” in this work.

Analysis of Variance (ANOVA) and Tukey-Kramer’s honestly significant difference (HSD) tests were performed between the three groups against the null hypothesis that there is no difference in mean stiffness with a significance (α) value of 0.05 using the commercially available software package JMP (JMP8.0, Cary, NC).

Clinical Feasibility

To test the clinical feasibility of our technique to measure parenchymal stiffness on patients with lung pathology, a single patient (male, age 64) with idiopathic pulmonary fibrosis (IPF) was recruited. This patient had pathologically proven Usual Interstitial Pneumonia (UIP) that was of mild to moderate severity on CT examination. MR Elastography was performed with the above mentioned parameters at RV and TLC. The data was compared to the data obtained for the volunteers. Because only one patient data set was acquired as part of this study, a test of statistical significance between normal and IPF lung stiffness was not performed.

Results

SE-MRE vs SE-EPIMRE

Representative right lung shear wave data obtained at end expiration from one of the healthy volunteers is shown in Figure 3 overlaid on the corresponding MR magnitude images. Data obtained with both the SE-MRE (Figure 3a) and SE-EPI MRE (Figure 3b) pulse sequences are shown and the similarity between the two datasets can be appreciated. The checkerboard pattern indicates regions with low phase-to-noise ratio (PNR), and it can be seen that regions away from the wave source exhibit increasingly lower PNR due to shear wave attenuation. The effective shear stiffness maps obtained from these datasets are also shown in Figure 3, and as expected appear very similar. The average effective stiffness obtained from the SE and SE-EPI MRE datasets are 3.6 (±0.63) kPa and 3.7 (±0.50) kPa, respectively. These data indicate that the newly developed SE-EPI MRE pulse sequence provides values consistent with those provided by the SE-MRE sequence. This is confirmed in Figure 3e, which shows excellent correlation between the effective stiffness values obtained from the SE and SE-EPI sequences at all three respiratory states.

Density Estimation

Figure 4 shows an example dataset obtained from the density estimation sequence (FGRE-LDE). This figure shows data obtained from the same volunteer at the same location as the data shown in Figure 3. Figure 4a shows the mean MR magnitude image used for the calculation of physical density at the lower TE (1.0 ms) and Figure 4b shows the corresponding image obtained at the relatively longer TE (1.8 ms). The reduction in the MR signal at the longer TE is visible. Figure 4c shows the density map obtained for the right lung overlaid on the MRE magnitude image. Figure 4d shows a profile of the mean density values from the anterior to the posterior lung, and demonstrates the gravity-induced gradual increase from the anterior to the posterior lung.

Validation Study

Figure 5 shows shear wave data obtained with the SE-EPI MRE sequence at all three respiration states (Figure 5a–c). It can be appreciated that lung area increases with increasing volume. Shear waves throughout the lungs are visible in all images, and demonstrate an increase in the shear wavelength with the increase in volume from RV to MID to TLC. The corresponding density maps shown in Figure 5 (Figure 5d–f) demonstrate

a reduction in density with increasing lung volume. The absolute shear stiffness maps calculated as the product of the effective stiffness and the density maps are shown in the right column (Figure 5g–i). Note the difference in the color maps between the effective stiffness values (Figure 3) and the absolute shear stiffness maps. From these data it can be seen that absolute stiffness values increase with the increasing lung volume.

Figures 6a–c show the effective stiffness, density, and absolute stiffness values at the three respiratory states for all five volunteers. Boxplots are overlaid on these points and the median values are connected with a line. While there was individual variability between the volunteers, the group values increased with increasing lung volume. The effective and absolute stiffness increases while density decreases with increasing volume from RV to TLC. Analysis of Variance of the absolute stiffness values indicate that the 3 groups were significantly different ($p = 1.82\times10^{-5}$). With the Tukey Kramer HSD method, the difference between the RV and MID absolute stiffness values was not significant. However, the pairwise difference between the other groups were statistically highly significant (RV - TLC: $p = 2.0\times10^{-5}$; MID - TLC: $p = 2.4\times10^{-4}$). The median densities were 0.27 g/cm^3, 0.20 g/cm^3 and 0.12 g/cm^3, and the median absolute stiffnesses were 0.90 kPa, 1.06 kPa and 1.55 kPa at RV, MID and TLC, respectively.

Clinical Feasibility

Figure 7 shows the shear wave data and absolute shear stiffness maps obtained from the patient volunteer at RV and TLC. Shear waves can be observed throughout the lungs and the increase in the shear wavelength at TLC compared to that at RV can be easily noted. The corresponding shear stiffness maps indicate that the stiffness does increase from RV to TLC. Note the change in the color map for these stiffness maps compared to the data shown for the volunteers. The mean shear stiffness values for this patient are indicated in Figure 7e. As expected, the stiffness of the diseased lung is greater than the stiffness values for the normal volunteers reported in this study.

Discussion

Proton MR Imaging of the lungs has been a challenging proposition due to the inherent low MR signal characteristics when compared to MR imaging of other, solid organs. The availability of novel hardware, contrast agents and pulse sequences provide opportunities to circumvent some of the limitations of MR-based lung imaging, and open new potential avenues for MR imaging of lung diseases [32–34]. One such application is the development of proton-based MRE of the lungs. It has been previously shown with a simple spin echo sequence modified to have a very short TE and sufficient motion sensitivity that the effective shear stiffness of human lung parenchyma can be quantified [25]. In this work, we have developed a fast SE-EPI MRE [35–37] sequence and have implemented a lung density estimation sequence to measure the absolute stiffness of the lung parenchyma. These techniques have been validated by quantifying an expected respiration dependent stiffness change in a series of 5 healthy volunteers. Clinical feasibility was demonstrated by quantifying lung parenchyma stiffness in a patient with known pulmonary fibrosis in which the lung is known to increase in stiffness compared to healthy lung.

Our data showed that effective stiffness (which is essentially the square of the shear wave speed) increases and the density decreased respectively with increasing lung volume from RV to TLC. The absolute shear stiffness value obtained as the product of effective stiffness and density did increase from RV to TLC, as expected. While there is no reference standard value for the measurement of stiffness of the lungs in vivo, the values obtained from our study at TLC were found to be in the range of previously reported shear modulus values obtained from various techniques [38, 39]. Specifically, our values at TLC were found to be consistent with the shear modulus of in vivo human lungs calculated using a recently developed ultrasound based surface wave measurement technique [40].

Stiffness values for each volunteer did increase from RV to MID to TLC. However, the group mean difference between the first two lung volumes was not statistically significant in our study of 5 volunteers. We believe that this discrepancy could be attributed to the choice of the MID volume level halfway between RV and TLC. While the stiffness is expected to increase with lung volume, the dependence will be nonlinear [1] and the increase in the shear stiffness will be lower in the low lung volumes and the change will accelerate at higher volumes. Also, the variability between the experimental MID volume levels and the expected MID volume levels (based on independent volumetric measurements, data not shown) indicate a need for better training and feedback systems, especially to obtain stiffness values at breath-held lung volumes that are not typical and are not easily reproducible.

There are several limitations to the current study. The first is that only 2D data sensitized to motion in a single direction were acquired for this study; for accurate estimation of the shear stiffness of the lung, full characterization of the complex 3D vector wave field is required. This is one of the motivations for the development of the EPI MRE pulse sequence described in this work. This MRE pulse sequence in combination with a surface coil array and parallel imaging techniques could potentially help in acquiring 3D vector lung MRE data in reasonable acquisition times. A second limitation of this methodology involves the process by which breath hold events are utilized for acquisition of data as this may prove to be technically challenging for patients with advanced lung disease. Clearly, clinical translation of this work will require further analysis of methodologies for implementation of respiratory triggering/gating into the SE-EPI MRE sequence. Another limitation of the study involves the presence of cardiac motion-induced artifacts which confound the data acquired from the left hemi thorax. This issue could be mitigated by the incorporation of cardiac triggering/gating. Also, areas of the lungs that are away from the wave source typically exhibited lesser shear wave amplitude (checker board pattern regions in figures 3, 5 and 7) due to significant wave attenuation. This issue is currently being investigated and could be reduced by using higher shear wave amplitude at the source or using multi-aspect drivers [9]. Finally, since the density estimation sequence is independently performed, misregistration issues could arise, which can potentially also be addressed by cardiac/respiratory triggered acquisitions.

In conclusion, the data obtained from this study confirm our hypothesis that the absolute shear stiffness of the lung could be imaged in vivo using a rapid SE-EPI MRE pulse sequence and a GRE-based localized density estimation sequence. It has also been shown in

healthy volunteers that the absolute shear stiffness increased with respiratory volume and that it is feasible to apply our technique on a patient with pulmonary fibrosis. These results identify the significant clinical potential of this technique and provide the motivation for ongoing research efforts to increase the flexibility and robustness of this approach.

Acknowledgments

This work was supported by NIH EB007593 and the Imaging Biomarker Discovery Program, Mayo Center for Individualized Medicine. The authors would also like to acknowledge the help of Kay Erickson with the spirometry measurements.

References

1. Suki B, et al. Biomechanics of the lung parenchyma: critical roles of collagen and mechanical forces. Journal of applied physiology. 2005; 98(5):1892–1899. [PubMed: 15829722]
2. Stamenovic D. Micromechanical foundations of pulmonary elasticity. Physiol Rev. 1990; 70(4): 1117–1134. [PubMed: 2217556]
3. Schaefer-Prokop C, et al. High-resolution CT of diffuse interstitial lung disease: key findings in common disorders. European Radiology. 2001; 11(3):373–392. [PubMed: 11288840]
4. Robertson HT, Buxton RB. Imaging for lung physiology: what do we wish we could measure? Journal of applied physiology. 2012; 113(2):317–327. [PubMed: 22582217]
5. Muthupillai R, et al. Magnetic resonance elastography by direct visualization of propagating acoustic strain waves. Science. 1995; 269(5232):1854–1857. [PubMed: 7569924]
6. Sack I, et al. Non-invasive measurement of brain viscoelasticity using magnetic resonance elastography. NMR in Biomedicine. 2008; 21(3):265–271. [PubMed: 17614101]
7. Sinkus R, et al. Viscoelastic shear properties of in vivo breast lesions measured by MR elastography. Magnetic resonance imaging. 2005; 23(2):159–165. [PubMed: 15833607]
8. Mariappan YK, Glaser KJ, Ehman RL. Magnetic resonance elastography: a review. Clinical anatomy. 2010; 23(5):497–511. [PubMed: 20544947]
9. Mariappan YK, et al. Magnetic Resonance Elastography with a phased array acoustic driver system. Magnetic resonance in medicine. 2009; 61(3):678–685. [PubMed: 19132758]
10. Elgeti T, et al. Cardiac Magnetic Resonance Elastography Toward the Diagnosis of Abnormal Myocardial Relaxation. Investigative Radiology. 2010; 45(12):782–787. [PubMed: 20829709]
11. Asbach P, et al. Viscoelasticity-based Staging of Hepatic Fibrosis with Multifrequency MR Elastography. Radiology. 2010; 257(1):80–86. [PubMed: 20679447]
12. Wuerfel J, et al. MR-elastography reveals degradation of tissue integrity in multiple sclerosis. Neuroimage. 2010; 49(3):2520–2525. [PubMed: 19539039]
13. Sahebjavaher RS, et al. Transperineal prostate MR elastography: Initial in vivo results. Magnetic Resonance in Medicine. 2013; 69(2):411–420. [PubMed: 22505273]
14. Garteiser P, et al. MR elastography of liver tumours: value of viscoelastic properties for tumour characterisation. European Radiology. 2012; 22(10):2169–2177. [PubMed: 22572989]
15. Green MA, et al. Measuring changes in muscle stiffness after eccentric exercise using elastography. Nmr in Biomedicine. 2012; 25(6):852–858. [PubMed: 22246866]
16. Cheng S, et al. Viscoelastic properties of the tongue and soft palate using MR elastography. Journal of Biomechanics. 2011; 44(3):450–454. [PubMed: 21040923]
17. Green MA, Bilston LE, Sinkus R. In vivo brain viscoelastic properties measured by magnetic resonance elastography. Nmr in Biomedicine. 2008; 21(7):755–764. [PubMed: 18457350]
18. Yin M, et al. Assessment of hepatic fibrosis with magnetic resonance elastography. Clinical Gastroenterology and Hepatology. 2007; 5(10):1207–1213. [PubMed: 17916548]
19. Wild J, et al. MRI of the lung (1/3): methods. Insights into imaging. 2012; 3(4):345–353. [PubMed: 22695952]

20. Maître, X., et al. Proceedings 17th Scientific Meeting, International Society for Magnetic Resonance in Medicine. Hawaii, USA: Honolulu; 2009. In vivo lung elastography with hyperpolarized helium-3 MRI.
21. Goss BC, et al. Magnetic resonance elastography of the lung: technical feasibility. Magnetic resonance in medicine. 2006; 56(5):1060–1066. [PubMed: 17036283]
22. Santarelli, R., et al. Proceedings 21st Scientific Meeting, International Society for Magnetic Resonance in Medicine. Salt lake city, USA: 2013. In vivo helium-3 MR-elastography: Assessment in small animal and human lungs.
23. McGee KP, Hubmayr RD, Ehman RL. MR elastography of the lung with hyperpolarized 3He. Magnetic resonance in medicine. 2008; 59(1):14–18. [PubMed: 18058936]
24. Cho A. Helium-3 Shortage Could Put Freeze On Low-Temperature Research. Science. 2009; 326(5954):778–779. [PubMed: 19892947]
25. Mariappan YK, et al. MR elastography of human lung parenchyma: technical development, theoretical modeling and in vivo validation. Journal of Magnetic Resonance Imaging. 2011; 33(6): 1351–1361. [PubMed: 21591003]
26. Mariappan YK, et al. Magnetic resonance elastography of the lung parenchyma in an in situ porcine model with a noninvasive mechanical driver: correlation of shear stiffness with trans-respiratory system pressures. Magnetic resonance in medicine. 2012; 67(1):210–217. [PubMed: 21590723]
27. Rump J, et al. Fractional encoding of harmonic motions in MR elastography. Magnetic Resonance in Medicine. 2007; 57(2):388–395. [PubMed: 17260354]
28. Manduca A, et al. Magnetic resonance elastography: non-invasive mapping of tissue elasticity. Medical image analysis. 2001; 5(4):237–254. [PubMed: 11731304]
29. Theilmann RJ, et al. Quantitative MRI measurement of lung density must account for the change in T2* with lung inflation. Journal of Magnetic Resonance Imaging. 2009; 30(3):527–534. [PubMed: 19630079]
30. Holverda S, et al. Measuring lung water: Ex vivo validation of multi-image gradient echo MRI. Journal of Magnetic Resonance Imaging. 2011; 34(1):220–224. [PubMed: 21698711]
31. Manduca A, et al. Spatio-temporal directional filtering for improved inversion of MR elastography images. Medical image analysis. 2003; 7(4):465–473. [PubMed: 14561551]
32. Ohno Y, et al. Dynamic oxygen-enhanced MRI reflects diffusing capacity of the lung. Magnetic resonance in medicine. 2002; 47(6):1139–1144. [PubMed: 12111960]
33. Takahashi M, et al. Ultra-short echo time (UTE) MR imaging of the lung: comparison between normal and emphysematous lungs in mutant mice. Journal of magnetic resonance imaging. 2010; 32(2):326–333. [PubMed: 20677258]
34. Hirsch S, et al. Measurement of vibration-induced volumetric strain in the human lung. Magnetic resonance in medicine. 2013; 69(3):667–674. [PubMed: 22529038]
35. Herzka DA, et al. Magnetic resonance elastography in the liver at 3 Tesla using a second harmonic approach. Magnetic Resonance in Medicine. 2009; 62(2):284–291. [PubMed: 19449374]
36. Murphy M, et al. Decreased brain stiffness in Alzheimer's disease determined by magnetic resonance elastography. Magnetic Resonance in Medicine. 2011; 34(3):494–498.
37. Mariappan, Y., et al. Proceedings 20th Scientific Meeting, International Society for Magnetic Resonance in Medicine. Melbourne, Australia: 2012. MR Elastography of Human Lung Parenchyma: Feasibility of Echo-Planar and Respiratory-Triggered Echo-Planar Imaging.
38. Lai-Fook SJ, Hyatt RE. Effects of age on elastic moduli of human lungs. Journal of applied physiology. 2000; 89(1):163–168. [PubMed: 10904048]
39. Hajji MA, Wilson TA, Lai-Fook SJ. Improved measurements of shear modulus and pleural membrane tension of the lung. Journal of applied physiology. 1979; 47(1):175–181. [PubMed: 468657]
40. Zhang X, et al. Noninvasive ultrasound image guided surface wave method for measuring the wave speed and estimating the elasticity of lungs: A feasibility study. Ultrasonics. 2011; 51(3):289–295. [PubMed: 20971489]

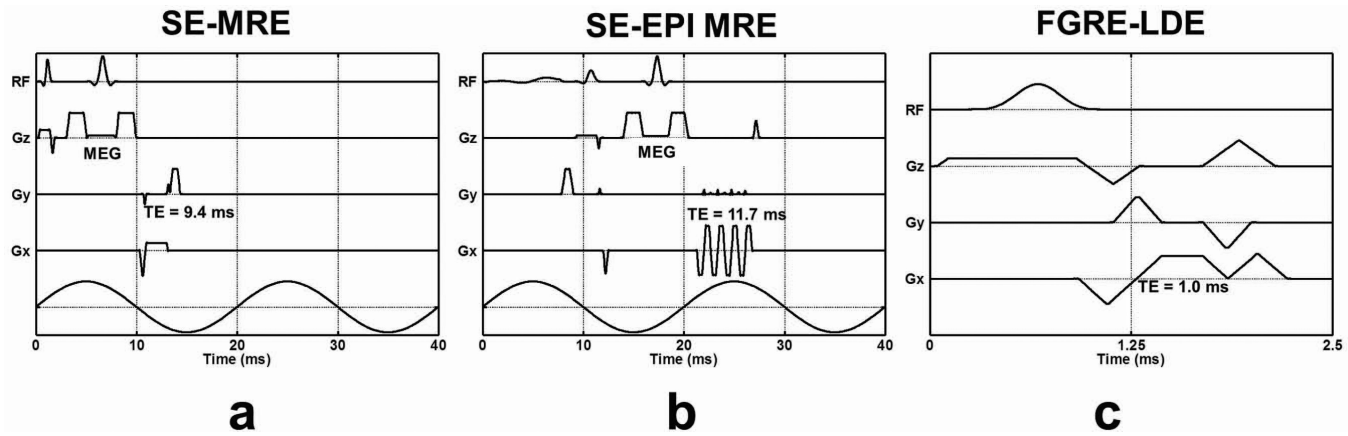

Figure 1. Pulse sequence Diagrams

(a) Pulmonaryspin echo MRE (SE-MRE) pulse sequence with two unipolar 2 ms MEG lobes. The TE was 9.4 ms. (b) Spin Echo EPI based MRE (SE-EPIMRE) pulse sequence with an echo train length of 8. The TE was 11.7 ms. (d) Fast GRE based pulse sequence used for lung density estimation; note the change in the time scale. The TE was 1.0 ms.

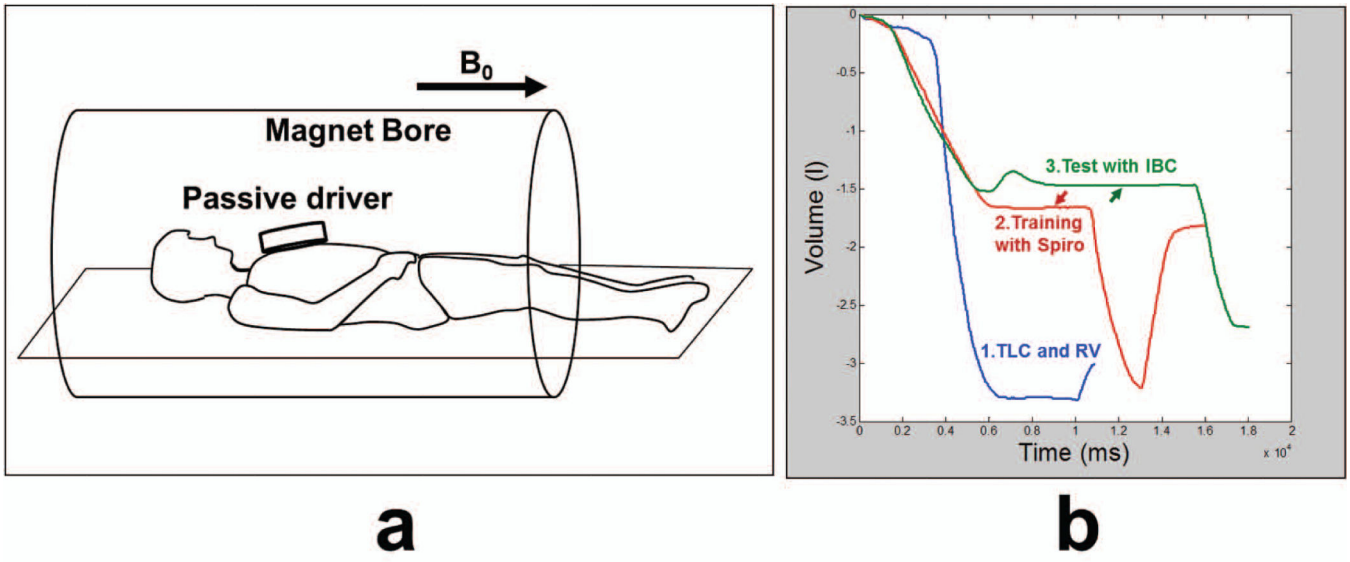

Figure 2. Experimental setup

(a) Subjects were positioned supine, the passive driver connected to the active driver was placed on the anterior chest wall creating continuous 50-Hz vibrations. (b) Spirometer tracings from a volunteer. This indicates that the MID respiratory volumes (arrows) maintained at the training step (red) and the interactive breath control calibrated step (green) were similar.

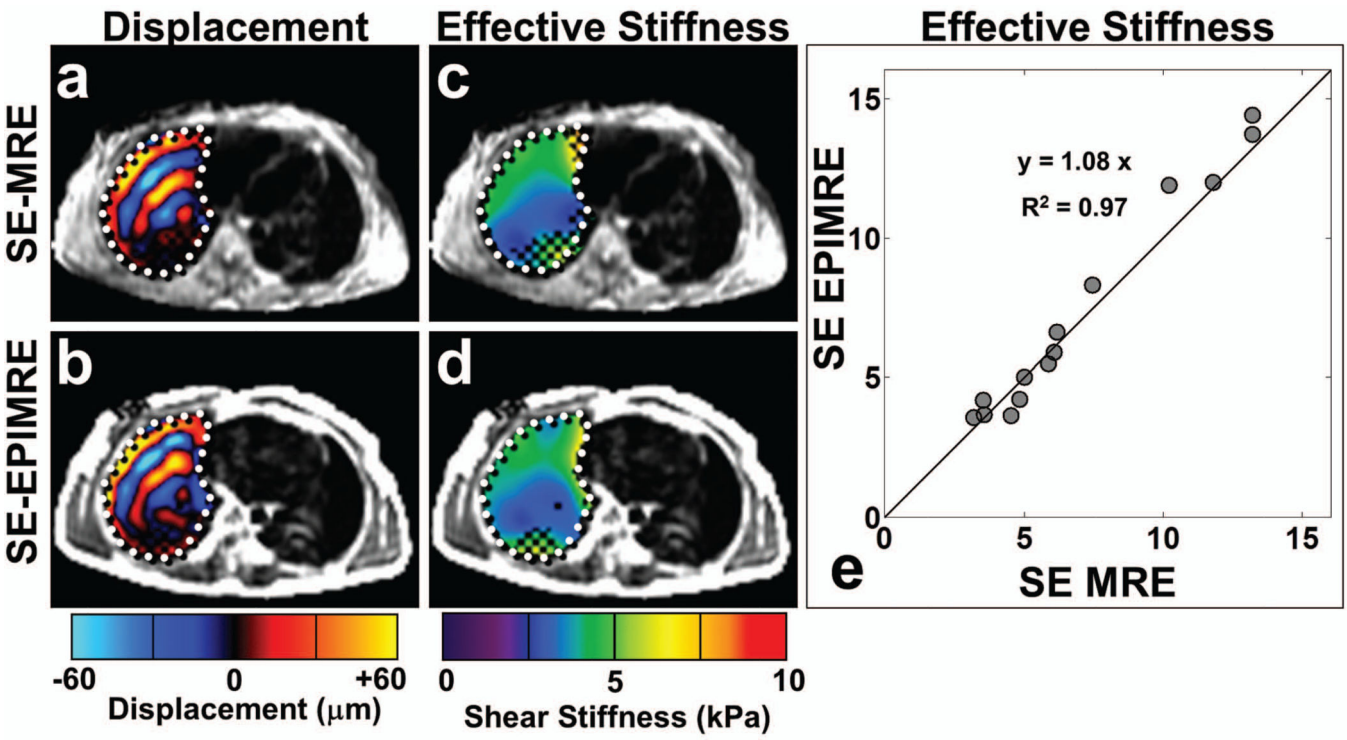

Figure 3. SE-MRE vs. SE-EPI MRE

Shear wave data at end expiration with (a) SE-MRE and (b) SE-EPI MRE. The similarity of the shear wave fields is apparent. The corresponding effective stiffness maps are shown in (c) and (d), respectively. The checker board pattern indicates regions with low wave amplitude. (e) The effective stiffness values obtained from SE-EPI MRE at the 3 respiratory states are plotted against the values obtained with SE MRE showing the significant correlation between the two measurements.

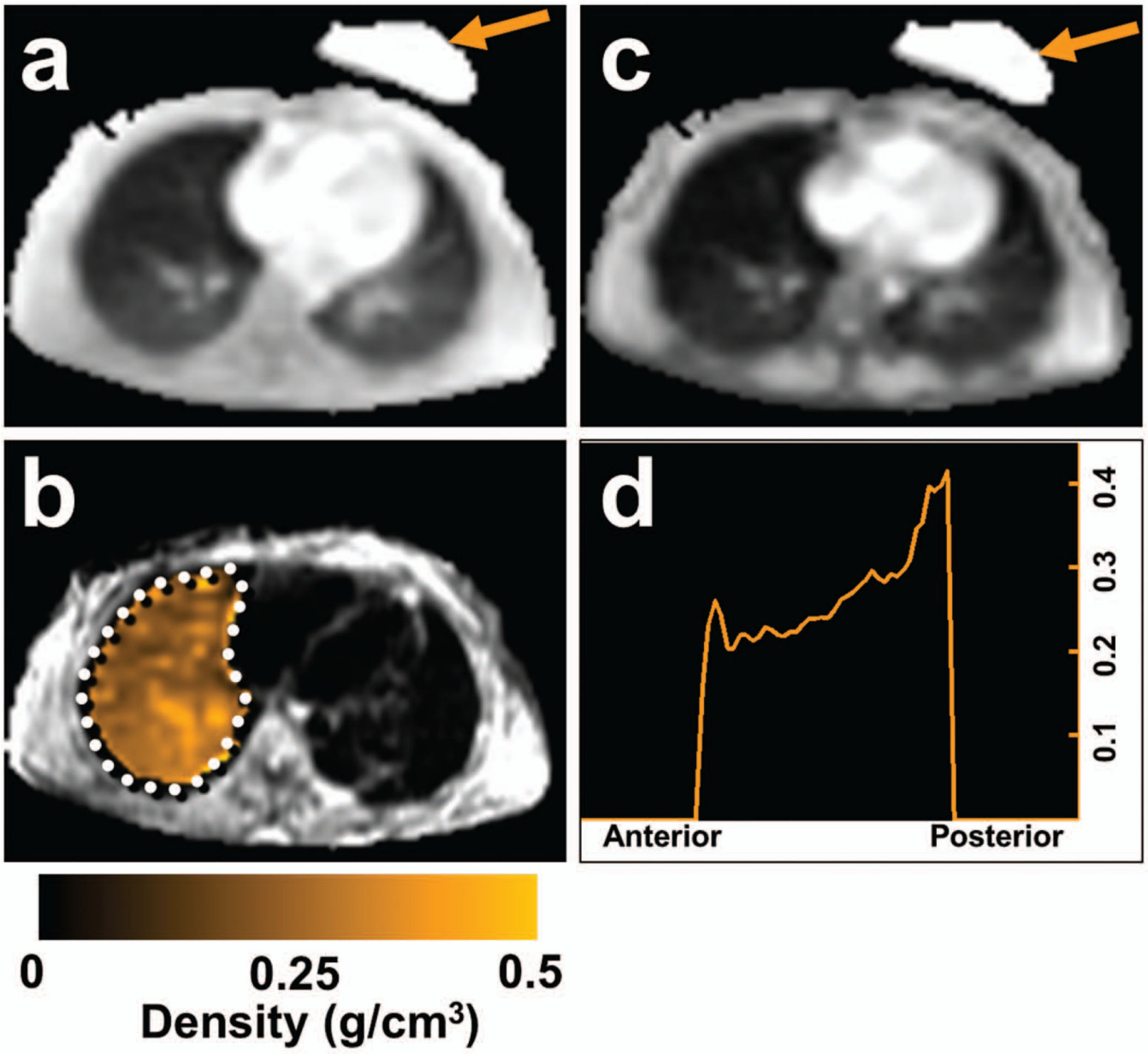

Figure 4. Density Estimation

Mean MR magnitude images calculated at (a) TE = 1.0 ms and at (b) TE = 1.8 ms for data obtained at end expiration. The reduction in signal at the higher TE, especially within the lungs, can be noted. The arrows indicate the gadolinium-doped water phantom whose signal was used for calibration purposes. (c) The corresponding density map overlaid on the MRE magnitude image. (d) Line profile indicating the mean density across the lung shows the presence of a gravity-dependent density gradient from the anterior (nondependent) to posterior (dependent) part of the lung.

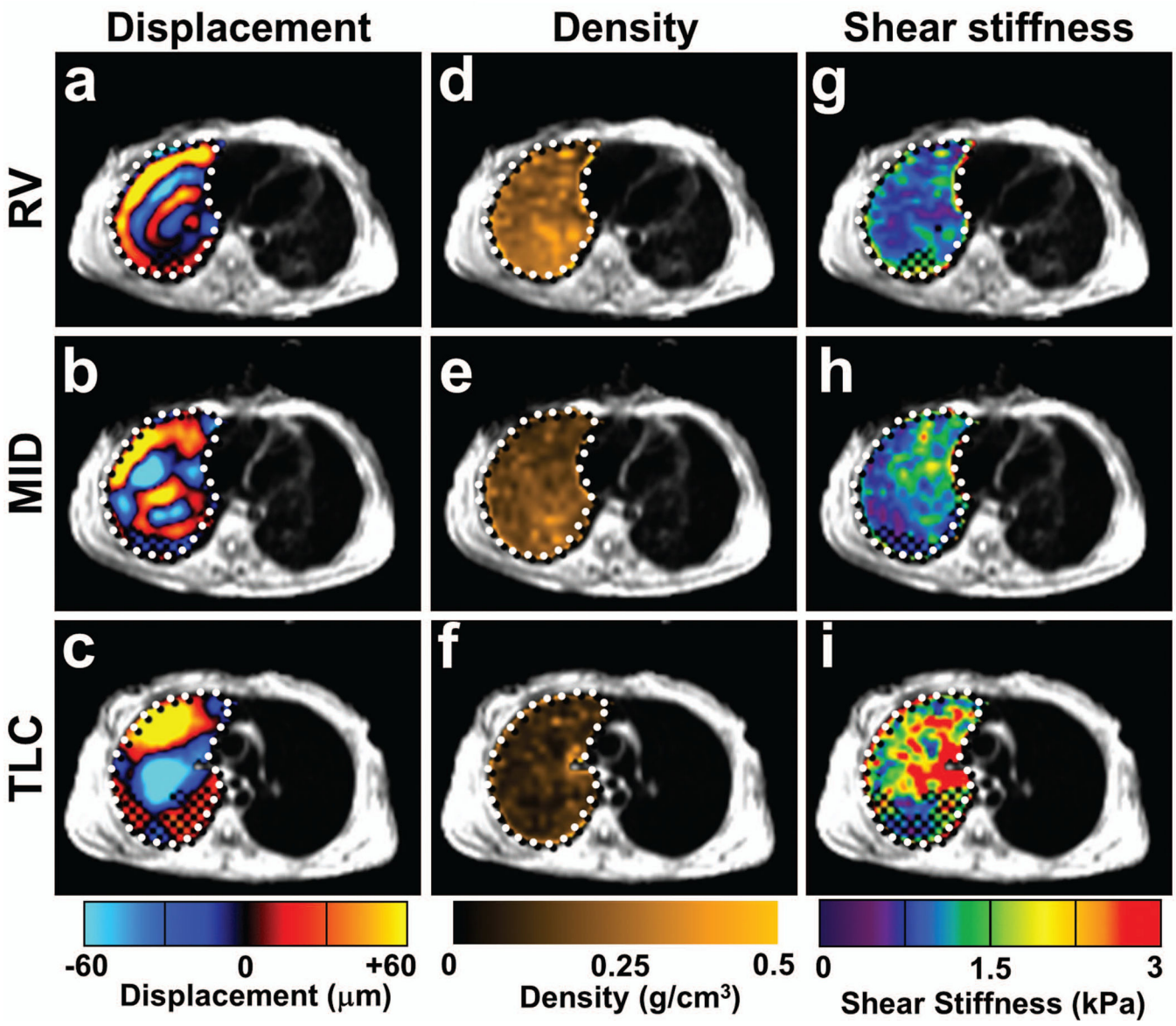

Figure 5. MRE data at RV, MID and TLC

(a,b,c). Shear wave displacement images, (d,e,f) tissue density maps and (g,h,i) absolute shear stiffness maps at RV, MID and TLC, respectively. The shear wavelength increases from RV to MID to TLC, but the corresponding density values decrease. The last column shows that the absolute shear stiffness increases with the increasing lung volume.

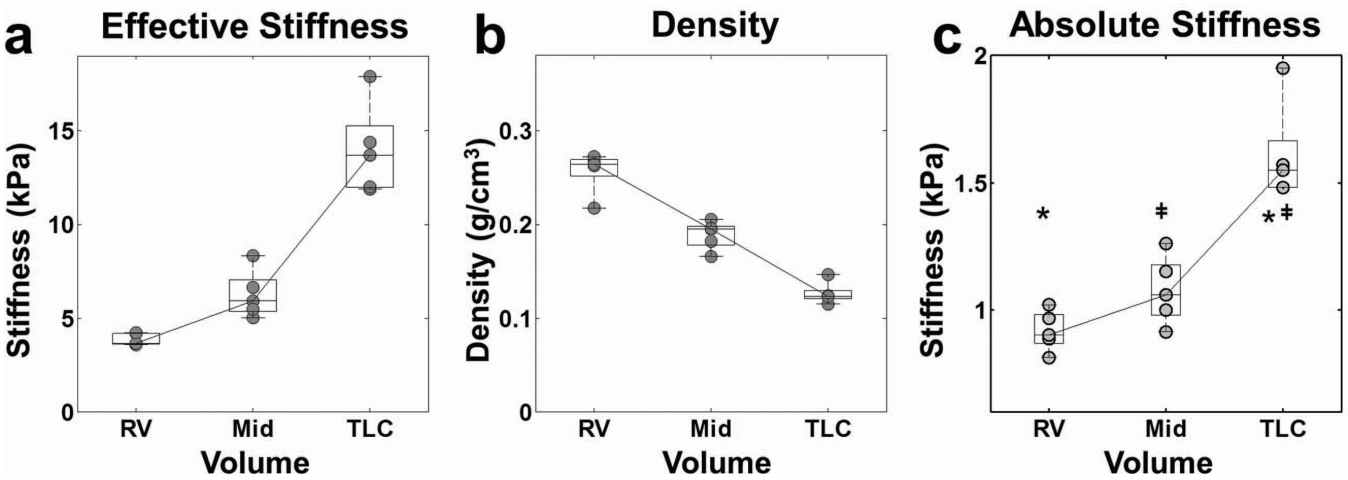

Figure 6. Validation study

(a) Effective stiffness, (b) density and (c) absolute shear stiffness values obtained from the five volunteers at the three respiratory states. Absolute stiffness pairwise group statistical significance is indicated with the asterisk (*) and the dagger (#). From the lines connecting the median values, the increase in the stiffness (both effective and absolute) and the decrease in the density with the increasing lung volume can be noted.

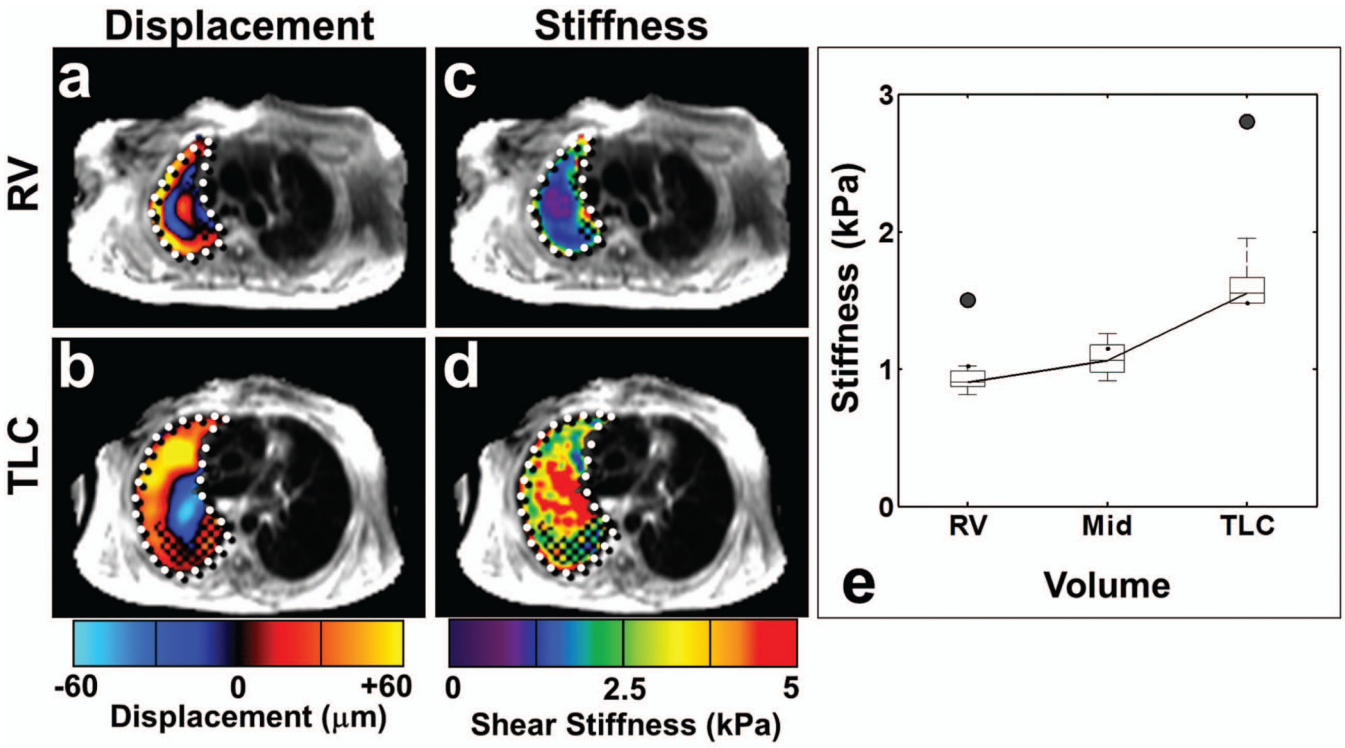

Figure 7. Clinical feasibility

Shear wave data obtained at (a) RV and (b) TLC. Corresponding absolute shear stiffness maps obtained at (c) RV and (d) TLC. The increase in the shear wavelength and shear stiffness is evident. (e) Shear stiffness values obtained from this patient are indicated with the solid dots. The values obtained from the healthy volunteers are indicated with the boxplots for reference and the increase in stiffness for the patient is visible.